R. & M. No. 3184
(19,504)
A.R.C. Technical Report

MINISTRY OF AVIATION

AERONAUTICAL RESEARCH COUNCIL
REPORTS AND MEMORANDA

The Effect of Reynolds Number on the Performance of a Single-Stage Compressor

By

A. D. S. CARTER, C. E. MOSS, G. R. GREEN and G. G. ANNEAR

LONDON: HER MAJESTY'S STATIONERY OFFICE
1960
PRICE 10*s*. 6*d*. NET

The Effect of Reynolds Number on the Performance of a Single-Stage Compressor

By

A. D. S. Carter, C. E. Moss, G. R. Green and G. G. Annear

Communicated by the Director-General of Scientific Research (Air), Ministry of Supply

Reports and Memoranda, No. 3184*

May, 1957

Summary.—The Reynolds-number effects on the performance of a single-stage compressor have been measured over the range $0{\cdot}08 \times 10^5$ to $9{\cdot}0 \times 10^5$. The tests were carried out in a variable-density return-circuit rig and the Reynolds number varied partly by fluid density and partly by speed.

The main conclusion arising from this work, and from an appreciation of other results is that the critical Reynolds number for a compressor blade is approximately $0{\cdot}5 \times 10^5$. This is about half the value previously assumed. Above the critical Reynolds number the efficiency variation can be expressed by the equation $(1 - \eta_{max}) = kR^{-0{\cdot}2}$.

In this region the fluid outlet angles and hence the stage temperature-rise coefficient remain constant.

Below the critical Reynolds number the efficiency can be expressed by $(1 - \eta_{max}) = kR^{-0{\cdot}5}$.

Some variation of the stage temperature-rise coefficient can occur in this region.

1. *Introduction.*—In a preliminary report[1] a description has been given of some tests on the effect of Reynolds number on the static-pressure rise through a single-stage axial-flow compressor. The work has since been extended and the full performance data of the compressor obtained over a wide Reynolds-number range. This report presents a comprehensive review of the results obtained in the complete test series.

The tests were carried out in the National Gas Turbine Establishment Variable-Density Return-Flow Rig. As description of the rig is beyond the scope of this report, a complete description of the rig and the operating technique will be issued as a separate report. A functional lay-out is shown in Fig. 1. A sectional drawing of the model test compressor is given in Fig. 2.

2. *Performance Measurements.*—2.1. *General.*—The measurements from which the performance of the compressor was calculated, comprised :

(*a*) Mass flow through test compressor.
(*b*) Static pressure between all blade rows.
(*c*) Compressor shaft torque input.
(*d*) Compressor speed.
(*e*) Rig pressure and temperature.

Measurement of the individual items is discussed in the following Sub-sections of the report.

* N.G.T.E. Report R.204, received 30th August, 1957.

2.2. *Mass-Flow Measurement.*—The mass flow was measured by a venturi meter situated in the fourth leg of the rig as shown in Fig. 1, and also by the test compressor intake. The venturi was calibrated by means of a pitot traverse at the throat with the diffusing section removed. The following discharge coefficients were obtained at various test Reynolds numbers :

*Venturi Reynolds number**	*Discharge coefficient*
$1{\cdot}26 \times 10^6$	0·999
$4{\cdot}58 \times 10^5$	0·998
$1{\cdot}65 \times 10^5$	0·997
$0{\cdot}94 \times 10^5$	1·000

* Based on venturi throat diameter.

This range covers that encountered in the compressor tests. A constant value of unity was taken for the discharge coefficient throughout this series of tests.

The compressor intake was also calibrated by a pitot traverse, though only at a blade Reynolds number of $1{\cdot}4 \times 10^5$. Traversing was carried out with the test compressor in position and running, but was limited by the number of instrument bosses which could be provided. A discharge coefficient of unity was obtained, and the mass flow measured in this way agreed with that obtained from the venturi to within 0·2 per cent. Subsequent comparison of the mass flow measured by the venturi and the compressor intake throughout the whole test series shows less good agreement. In general, the agreement is within $\pm$ 2·0 per cent, but there were some examples, particularly at low flows, showing discrepancies of $\pm$ 4·0 per cent.

2.3. *Pressure Measurement.*—The static pressure at any plane was measured by means of eight equi-spaced wall static tappings on both the inner and outer annulus walls. The tappings were 0·030-in. diameter. There were measuring stations before the inlet guide vanes, between each of the blade rows, and after the stator, as shown in Fig. 2. Each of the statics was connected to a tube of a multi-tube manometer to record each pressure individually. In addition, each static tapping of a bank was taken to an averager and the mean value of the static pressure at each station recorded directly on the manometer. A similar arrangement was adopted for the venturi.

The pressures were measured by vertical multi-tube manometers filled with oil or mercury as necessary. At the lower end of the speed range the pressures were very small and a 40-way multi-tube sloping manometer giving a magnification of 10/1 was employed. All the manometers were calibrated against a Betz manometer.

Total pressures were not normally measured in this series of tests since this would have involved extensive traversing. The total pressure at any station was calculated from the measured static pressure and the mean dynamic pressure estimated from the measured mass flow.

2.4. *Compressor Torque Measurement.*—The system used for torque measurement is illustrated in principle in Fig. 3. The compressor shaft bearings are carried in a tube on which is mounted the driving turbine stator system. An auto-setting weighbeam measures the thrust from a torque arm which is mounted on the tube. As shown in Fig. 3, all swirl in the air supply to and the discharge from the turbine is removed by honeycomb straighteners. The torque reaction on the tube is thus equal to the compressor-rotor aerodynamic torque, including disc windage.

Although simple in principle, the commissioning of the torque measuring system proved troublesome and lengthy. The subject is really outside the scope of this report and will be treated in detail in the report on the rig. In its final state the system proved reliable and consistent. The only unsatisfactory feature was a zero error, *i.e.*, when the turbine was run with the compressor removed a negative torque was recorded. This torque remained consistent at any speed. It is suspected that the zero error is due to thermal distortion, possibly of the swung tube, due to heat from the bearings under running conditions. The error was determined by driving the

turbine and shaft without the compressor at various speeds. The steady observed torque is then added to that recorded during a compressor test at the same speed. The error is small but is tabulated in Appendix I for record purposes.

A further zero error can occur when continuous testing is carried out over a pressure range. Due to movement of the rig under pressure a spurious load is imposed on the weighbeam. Its value has been recorded in Appendix I for reference. The correction to be applied is small. When determining the normal constant-speed characteristic at a fixed tunnel pressure the same correction appears in both the static and running torque and is therefore neglected.

2.5. *Speed Measurement.*—The method adopted for measuring torque ruled out any direct mechanical drive for recording speed. A magnet was therefore fixed to the turbine rotor disc. This excites eight equi-spaced iron-cored coils held on the turbine stator casing.

For roughly setting speed a Maxwell-type speed indicator is used, but speed is finally controlled by comparing the coil output frequency with a standard 1,000 c.p.s. fork. This gives a very accurate indication of any speed variation. A certain amount of speed drift was noted during running, but speed variations during steady running were probably limited to $\pm$ 10 r.p.m.

2.6 *Rig Temperature and Pressure Measurement.*—Neither rig temperature nor pressure measurement presented any serious difficulty. Temperature was measured by a 24-ft long copper-cased nickel wire resistance thermometer which was fitted to the 24-in. inlet section in an equi-spaced spiral. It is shown in Fig. 2. The rig datum pressure was measured relative to atmosphere by an ordinary mercury in glass U manometer.

2.7. *General Accuracy of Results.*—In all, the test programme recorded in this report lasted approximately one year. During the course of the programme it became our practice to repeat a test at 7,500 r.p.m. with a rig pressure of 1 Atm as a datum. No significant change was ever observed in this characteristic. In addition, all tests were repeated at least once, and sometimes more, over a wide interval of time. The reader is able to judge the repeatability of the tests from the results presented. It is not possible to compare the static-pressure characteristics presented in this report with those given in Ref. 1. In the latter case the static pressure was measured at the outside annulus wall only, whereas for these tests measurements were made at both inside and outside walls, a mean value being taken since a static-pressure gradient was usually present. Several comparisons were made using the readings at the outside wall only, and in all cases good agreement was obtained between both series of tests.

As a check on the absolute accuracy, the temperature rise across the compressor was measured directly by means of thermo-couples which were traversed after the stator. This was compared with the temperature rise calculated from the torque measurements. The comparative results have been tabulated in Appendix II. In Fig. 4 the equivalent temperature rise at 7,500 r.p.m. has been plotted against flow coefficient. It will be seen that the error is systematic. Agreement is very good in the middle of the flow range when a uniform temperature rise was obtained at all radii. Towards the ends of the flow range considerable temperature striation was recorded as shown in Fig. 5. In these circumstances agreement between torque and direct temperature measurement was not so good. The authors are convinced that the overall torque is much more reliable in these circumstances, providing a completely inherent integration of the radial work variation. Any further attempts to measure the temperature directly were therefore abandoned. It was considered that the agreement obtained at the uniform flow conditions had proved the absolute accuracy of the torque measuring system. This agreement, incidentally, provided a further check on the accuracy of the mass-flow measurement.

A check was also made on the indirect method adopted for total-head pressure-rise variation. This was done by traversing with a pitot comb. It was found that the efficiency so obtained was some 1·5 per cent higher than that obtained from the routine method. Some of the effect may be due to a contraction effect similar to that encountered in cascade wind-tunnel work. On the other hand traversing was confined to a relatively small sector of the annulus, so some error may arise from that source.

No direct measurements of the turbulence level were made either in these tests or in those presented in Ref. 1. However, the approach section is very similar to that usually employed in compressor testing and so the turbulence level may be taken the same as that at the first stage of a multi-stage compressor operating under normal conditions.

3. *Details of Test Compressor Stage.*—The test compressor is an aerodynamic model of the first stage of the N.G.T.E. Serial Number 109 Compressor. This is a high-duty compressor giving a pressure ratio of 4·5/1 in six stages. The single-stage model was scaled down from 24·34 in. outside diameter to 10 in., but relatively larger blade chords were used to keep down the bending stress at the higher air densities. The design speed of the model is 23,100 r.p.m., but it is stressed for 20 per cent overspeed. The salient design details of the model are :

Mass flow	= 12·5 lb/sec
Speed	= 23,100 r.p.m.
Temperature rise	= 29 deg C (Ω = 1·0)
Blade twist	= Constant α_3
Outlet angle (α_2)	= 25·6 deg
Mean blade speed	= 812 ft/sec
Diameter ratio at inlet to rotor	= 0·6
Blade profile	= C.4
Blade camber-line	= P.40

Full design and inspection details of the model are given in Appendix III.

4. *Test Procedure and Reduction of Results.*—The general operating conditions that can be obtained in the rig have been illustrated in Fig. 6, which has been taken from Ref. 1. In carrying out this series of tests the same path was followed as in the earlier tests of Ref. 1. It covered the Reynolds-number range $0{\cdot}08 \times 10^5$ to 9×10^5, and is denoted by the crosses in Fig. 6. Normal constant-speed characteristics were taken at fixed tunnel densities covering the Reynolds-number range in multiples of $\sqrt{2}$. In addition, variable density tests were run at the peak efficiency points, the required flow being obtained from the constant-speed characteristic. Actually it was found that a constant-compressor-load throttle setting gave a close enough approximation over a reasonable Reynolds-number range.

The test performance is presented by the non-dimensional flow coefficient, the non-dimensional pressure rise, and efficiency. Following the convention adopted in the previous series of tests all the results have been referred to the mid-plane of the rotor.

Also following the convention adopted in the previous series of tests the Reynolds numbers quoted throughout this report are based on blade chord and mean-diameter blade speed. The relationship between this Reynolds number and that based on inlet fluid velocity is plotted in Fig. 7. For all practical purposes they are identical for this compressor.

5. *Reynolds-Number Effects.*—5.1. *Test Results.*—The characteristics that were obtained have been plotted out in full in Figs. 8 to 21. Of primary interest is the variation in peak stage efficiency with Reynolds number, and this has been further illustrated in Fig. 22. Here the peak efficiencies determined from the characteristics, together with those measured in the constant-throttle runs, have been plotted against Reynolds number on a logarithmic basis. It will be seen that the points lie substantially on two straight lines, with a critical at a Reynolds number of $0{\cdot}45 \times 10^5$. Above and below the critical Reynolds number the efficiency variation can be expressed by the following relationships :

$$(1 - \eta_{max}) = kR^{-0{\cdot}2} \text{ for } R > 0{\cdot}45 \times 10^5 \quad \ldots \quad (1)$$

$$(1 - \eta_{max}) = kR^{-0{\cdot}5} \text{ for } R < 0{\cdot}45 \times 10^5 \ldots \quad \ldots \quad (2)$$

Above the critical Reynolds number the viscosity effects have been confined entirely to drag and thus to the stage efficiency. The stage temperature-rise coefficient remained constant as can be seen from Fig. 23. This was also confirmed by some traverses of the fluid outlet angle at the mean diameter from the stator shown in Fig. 24. With a predominantly turbulent boundary layer little breakaway would occur at the peak-efficiency point. The fluid outlet angle would thus be practically equal to that calculated in potential flow and constant. Hence a constant-stage temperature-rise coefficient is to be expected in this region, with Reynolds-number effects confined to drag. It is, however, a little surprising that the stage drag should follow the same law as the drag on a flat plate since nearly half the stage drag is due to secondary losses.

Below the critical Reynolds number the rapid increase of drag is due presumably to transition to laminar boundary-layer flow, and, at the high lift coefficients at which these blades have to operate, laminar separation. In this Reynolds-number range the drag follows approximately a half power law. In the laminar-flow region the temperature-rise coefficient does not remain constant, as can be seen from Fig. 23. The variation is small and is an increase rather than the expected decrease. The mean measured fluid outlet angle from the stator remained almost unchanged down to the lowest Reynolds number tested.

At flows other than that giving maximum efficiency the relationships (1) and (2) still hold approximately, but no reliable variation can be obtained for the low-efficiency flow conditions. These are of little practical interest, however.

5.2. *Discussion of Results.*—Perhaps the most surprising feature of the results is the low critical Reynolds number which has been recorded. A value of 1×10^5 is often quoted for compressor blades. This value is based largely on cascade results and is certainly a good mean value in that instance. The higher degree of turbulence present in a compressor could easily account for a factor of two in the critical Reynolds number, so no great significance should be attached to this discrepancy. In this connection it is interesting to note that the inlet guide vanes, which are not preceded by any previous blade row, apparently have a critical at 1×10^5 in these single-stage tests. This can be seen from Fig. 25 where the static-pressure drop across this blade row has been plotted against Reynolds number. It is to be noted that the inlet guide vanes will be operating at low lift coefficients, hence laminar separation is not likely. A lower drag, and hence pressure drop, is to be expected for a laminar boundary layer, *i.e.*, at the lower Reynolds numbers.

A comparison of all compressor results[2, 3, 4, 5] known to the authors has been made in Fig. 26. It would seem that the case for a critical value at 1×10^5 can hardly be made from these results and must lie heavily on the cascade data. The majority of compressor results are not very detailed, and a certain amount of latitude is available in selecting the critical value. However, the authors put considerable reliance on the present series of tests. Taken in conjunction with the other results they would favour a lower value for the critical than has been assumed in the past. It must be pointed out, however, that the blades used in these tests had parabolic-arc camber-lines. Cascade tests reported in Ref. 7 suggest that this type of blade has a lower critical Reynolds number than those with the more popular circular-arc camber-line. On the other hand the collected results in Fig. 26 include tests on circular-arc cambered blades. Additionally, the pressure measurements on three compressors having circular-arc cambered blades given in Ref. 6 show no indication of a critical down to a Reynolds number of $0{\cdot}4 \times 10^5$. A critical value of the Reynolds number nearer $0{\cdot}5 \times 10^5$ would seem to be more appropriate for compressor blades on the basis of the evidence collected. Considerable weight has been placed on the single-stage results, but it is unlikely that a stage in a multi-stage machine will have a higher critical due to the high turbulence. The Reynolds-number effects on a multi-stage compressor will, of course, be the aggregate of the effects on the individual stages.

A further common discrepancy between cascade and compressor test results is the variation of the outlet angle below the critical Reynolds number. Cascade tests always show (*see* Refs. 7 and 8, for example) a very sharp change, whereas compressor test results show little variation

in outlet angle and consequently in the non-dimensional temperature-rise coefficient. These tests did show some slight variation in the non-dimensional temperature rise as shown in Fig. 23, but traverses of the fluid outlet angle after the stator reproduced in Fig. 24 show no critical effects.

6. *Conclusions.*—The main conclusion arising from this work, and from an appreciation of other results is that the critical Reynolds number for a compressor blade is approximately $0{\cdot}5 \times 10^5$. This is about half the value previously assumed. Above the critical Reynolds number the efficiency variation can be expressed by the equation

$$(1 - \eta_{\max}) = kR^{-0{\cdot}2}.$$

In this region the fluid outlet angles and hence the stage temperature-rise coefficient remain constant.

Below the critical Reynolds number the efficiency can be expressed by

$$(1 - \eta_{\max}) = kR^{-0{\cdot}5}.$$

Some variation of the stage temperature-rise coefficient can occur in this region.

REFERENCES

No.	Author	Title, etc.
1	A. G. Smith, C. E. Moss, R. D. Pearson and G. R. Green	Measurements of the static pressure rise in a single-stage fan at low Mach numbers over a wide range of Reynolds Number. (Unpublished M.o.S. Report.)
2	L. E. Wallner and W. A. Fleming ..	Reynolds-number effect on axial-flow compressor performance. N.A.C.A. Research Memo. E.9 G.11.
3	J. Lalive d'Epinay	Aerodynamic methods applied to turbo-machine research. *Brown Boveri Review*. Vol. 37. p. 357. 1950.
4	A. L. Ponomareff	Axial-flow compressors for gas turbines. *Trans. A.S.M.E.* Vol. 70. p. 295. 1948.
5	R. A. Jeffs	Preliminary note on the performance of axial compressor blading designed to operate in a radially varying axial velocity distribution. (Unpublished M.o.S. Report.)
6	S. J. Andrews and H. Ogden	A detailed experimental comparison of axial compressor blades designed for free vortex flow and equivalent untwisted and twisted constant-section blading. R. & M. 2928. July, 1953.
7	H. G. Rhoden	Effects of Reynolds number on the flow of air through cascades of axial-flow compressor blades. Report of Engineering Department, Cambridge University. June, 1952.
8	T. V. Lawson	Investigation into the effect of Reynolds number on cascades of blades with parabolic-arc camber-lines. (Unpublished M.o.S. Report.)

APPENDIX I

Torque Measurement—Zero Errors

(*a*) Zero error due to negative torque recorded when running turbine and shaft system alone.

Speed (r.p.m.)	Zero error* (Units†)	Average torque recorded in tests (Units† at $\frac{1}{4}$ Atm)
3,750	2	50
5,000	3	90
7,500	$4\frac{1}{3}$	200
10,000	$7\frac{1}{3}$	350
12,500	9	550
15,000	$14\frac{1}{3}$	800
17,500	20	1,000
20,000	23	

* Zero error to be added to recorded torque to obtain true torque.

† 1 unit = 0·00666 ft lb.

(*b*) Zero error due to movement of rig under pressure.

Rig pressure (in. Hg gauge)	Zero error§ (Units)
20	0
40	$1\frac{1}{3}$
60	$2\frac{1}{3}$
80	$6\frac{2}{3}$
100	10
120	$17\frac{1}{3}$

§ Zero error to be subtracted from recorded torque to obtain true torque.

N.B.—This correction is only applied during a varying density run.

APPENDIX II

Comparison of Temperature Rise Calculated from Torque and Mass Flow Readings with that Measured by Thermo-couples

Speed 7,500 *r.p.m., rig pressure* 1 *Atm (nominal)*

Flow coefficient	0·495	0·567	0·609	0·695	0·748	0·755	0·907
ΔT from torque .. ..(deg C)	3·42	3·10	2·97	2·60	2·29	2·24	1·46
ΔT from thermocouples (deg C)	3·12	3·18	3·17	2·61	2·26	2·21	1·19
Difference .. .. ..(deg C)	0·30	0·08	0·20	0·01	0·03	0·03	0·27

Speed 10,000 *r.p.m., rig pressure* 1 *Atm (nominal)*

Flow coefficient	0·593	0·609	0·700	0·797
ΔT from torque ..(deg C)	5·49	5·33	4·63	3·72
ΔT from thermocouples (deg C)	5·71	5·27	4·61	3·62
Difference .. ..(deg C)	0·22	0·06	0·02	0·10

Speed 17,500 *r.p.m., rig pressure* $1/(2\sqrt{2})$ *Atm (nominal)*

Flow coefficient	0·664	0·744	0·748
ΔT from torque .. ..(deg C)	14·28	12·15	12·32
ΔT from thermocouples (deg C)	14·68	12·05	12·01
Difference .. ..(deg C)	0·40	0·10	0·31

APPENDIX III

Dimensions of the Test Model

The complete list of nominal dimensions is shown in the table below :

	I.G.V.		Rotor		Stator	
	In	Out	In	Out	In	Out
Inner diameter of annulus (in.)	5·67	5·93	6·01	6·30	6·42	6·72
Mean diameter of annulus (in.)	7·83	7·96	8·00	8·15	8·21	8·36
Outer diameter of annulus (in.)	10·00	10·00	10·00	10·00	10·00	10·00
Diameter of inner blade section (in.)	6·302		6·492		6·878	
Diameter of mean blade section (in.)	7·946		8·054		8·316	
Diameter of outer blade section (in.)	9·588		9·616		9·754	
Inner blade angles (deg)	0·00	−15·68	45·2	6·00	48·39	13·59
Mean blade angles (deg)	0·33	−25·67	49·2	20·51	48·71	20·86
Outer blade angles (deg)	0·00	−36·33	53·04	34·84	48·94	28·04
Inner camber angles (deg)	15·68		39·20		34·80	
Mean camber angles (deg)	26·00		28·70		27·85	
Outer camber angles (deg)	36·33		18·20		20·90	
Inner stagger angle (deg)	10·50		−18·30		−24·40	
Mean stagger angle (deg)	17·75		−29·30		−29·38	
Outer stagger angle (deg)	25·00		−40·30		−34·36	
s/c inner	0·94		0·66		0·65	
s/c mean	1·19		0·82		0·78	
s/c outer	1·44		0·97		0·92	
Chord, everywhere (in.)	1·00		1·00		1·00	
Number of blades	21		31		34	
t/c inner (per cent)	9·0		11·0		8·0	
t/c mean (per cent)	9·0		9·0		9·0	
t/c outer (per cent)	9·0		7·0		10·0	
Throat/pitch A_t/s inner	0·89		0·73		0·74	
Throat/pitch A_t/s mean	0·87		0·74		0·74	
Throat/pitch A_t/s outer	0·82		0·70		0·72	
Deviation angle, mean (deg)	2·84		5·06		4·83	
Air outlet angle, mean (deg)	−22·83		+25·57		+25·69	
Blade speed *U* inner (ft/sec)	0		654·75		0	
Blade speed *U* mean (ft/sec)	0		812·22		0	
Blade speed *U* outer (ft/sec)	0		969·70		0	

Inspection of the model was by measurement of blade throats and stagger angles at three radial stations ; all blade profiles were inspected by projection when being manufactured. The deviations from nominal dimensions are shown below :

I.G.V.—21 Blades

Section diameter (in.)	6·302	7·946	9·588
Nominal A_t/c	0·836	1·02	1·18
Measured mean	0·846	1·050	1·197
Variation	+0·006	+0·017	+0·009
	−0·011	−0·013	−0·013
Nominal stagger	10° 30′	17° 45′	25° 0′
Measured mean	10° 36′	18° 32′	25° 11′
Variation	+27′	+33′	+51′
	−28′	−37′	−49′

APPENDIX III—*continued*

Rotors—31 Blades

Section diameter (in.) ..	6·492	8·054	9·616
Nominal A_t/c	0·482	0·607	0·686
Measured mean	0·488	0·602	0·684
Variation	+0·009	+0·009	+0·012
	−0·009	−0·008	−0·011
Nominal stagger	−18° 18′	−29° 18′	−40° 18′
Measured mean	−17° 30′	−28° 06′	−39° 08′
Variation	+23′	+38′	+43′
	−17′	−22′	−32′

Stators—34 Blades

Section diameter (in.) ..	6·878	8·316	9·754
Nominal A_t/c	0·467	0·565	0·643
Measured mean	0·480	0·579	0·669
Variation	+0·007	+0·006	+0·005
	−0·010	−0·003	−0·009
Nominal stagger	−24° 24′	−29° 23′	−34° 22′
Measured mean ..	−23° 42′	−28° 46′	−33° 55′
Variation	+45′	+54′	+53′
	−30′	−36′	−32′

Axial Dimensions and Annulus Areas

Axial positions are given relative to the bullet flange shown on the left-hand side of Fig. 2.

	Axial position (in.)	Inner diameter (in.)	Area (ft²)	Tip clearance (in.)
'E' plane..	2·395	6·998	0·2784	
Mid. ht. O.G.V. T.E. ..	2·959	6·926	0·2838	0·031 to 0·045
Mid. ht. O.G.V. L.E. ..	3·951	6·720	0·2911	
'D' plane	4·293	6·643	0·3047	
Mid. ht. stator T.E. ..	4·755	6·543	0·3119	0·026 to 0·046
Mid. ht. stator L.E. ..	5·613	6·356	0·3252	
'C' plane	6·195	6·274	0·3308	
Mid. ht. rotor T.E. ..	Approximately central to B and C planes			0·015 to 0·020
Mid. ht. rotor L.E. ..				
'B' plane..	7·493	5·974	0·3508	
I.G.V. T.E. Mid. ht. ..	8·100			0·011 to 0·019
I.G.V. L.E. Mid. ht. ..	9·048			
'A' plane..	9·602	5·602	0·3742	
	Model O.D. constant at 10·00 in.			

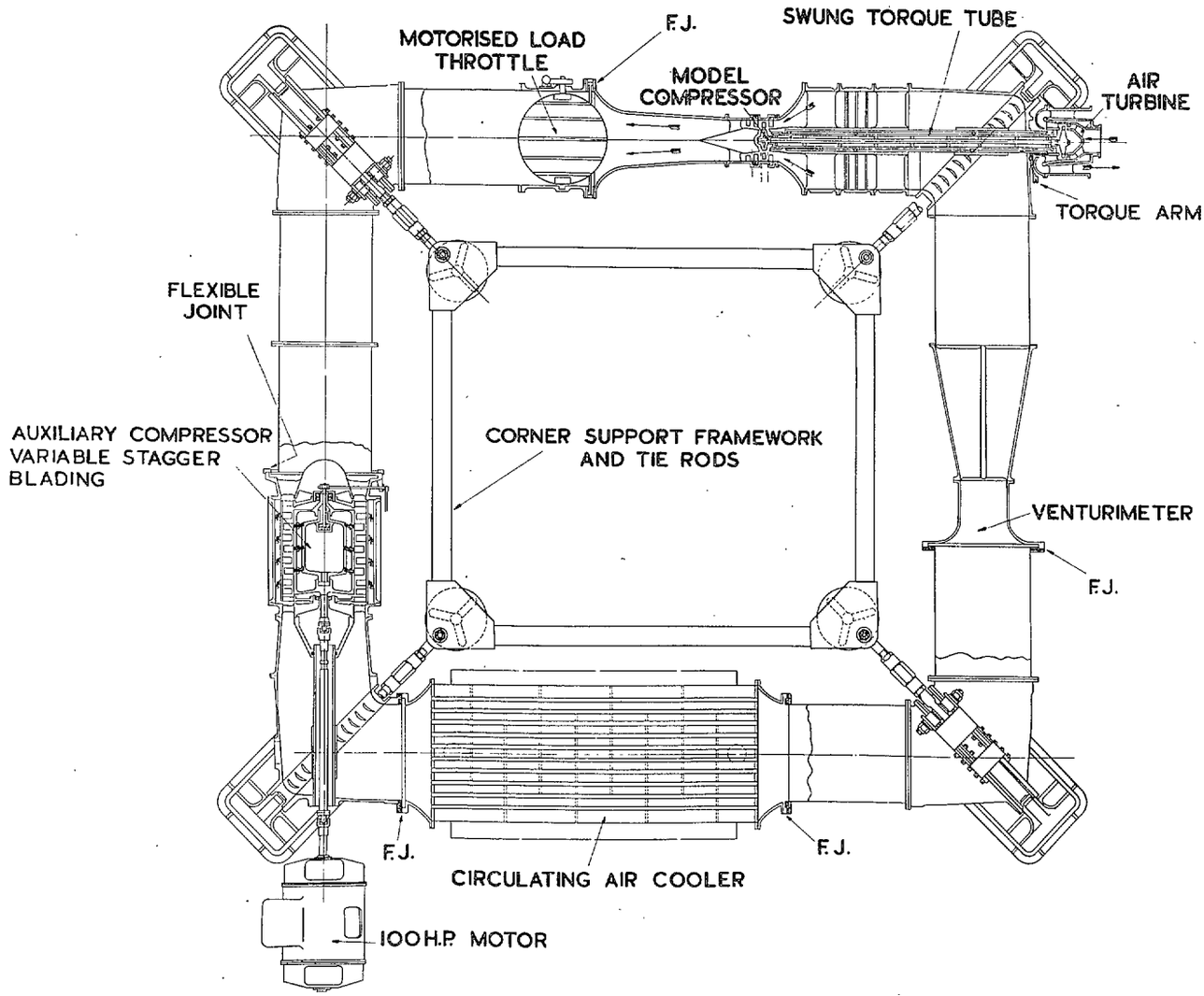

FIG. 1. Variable-density compressor test tunnel.

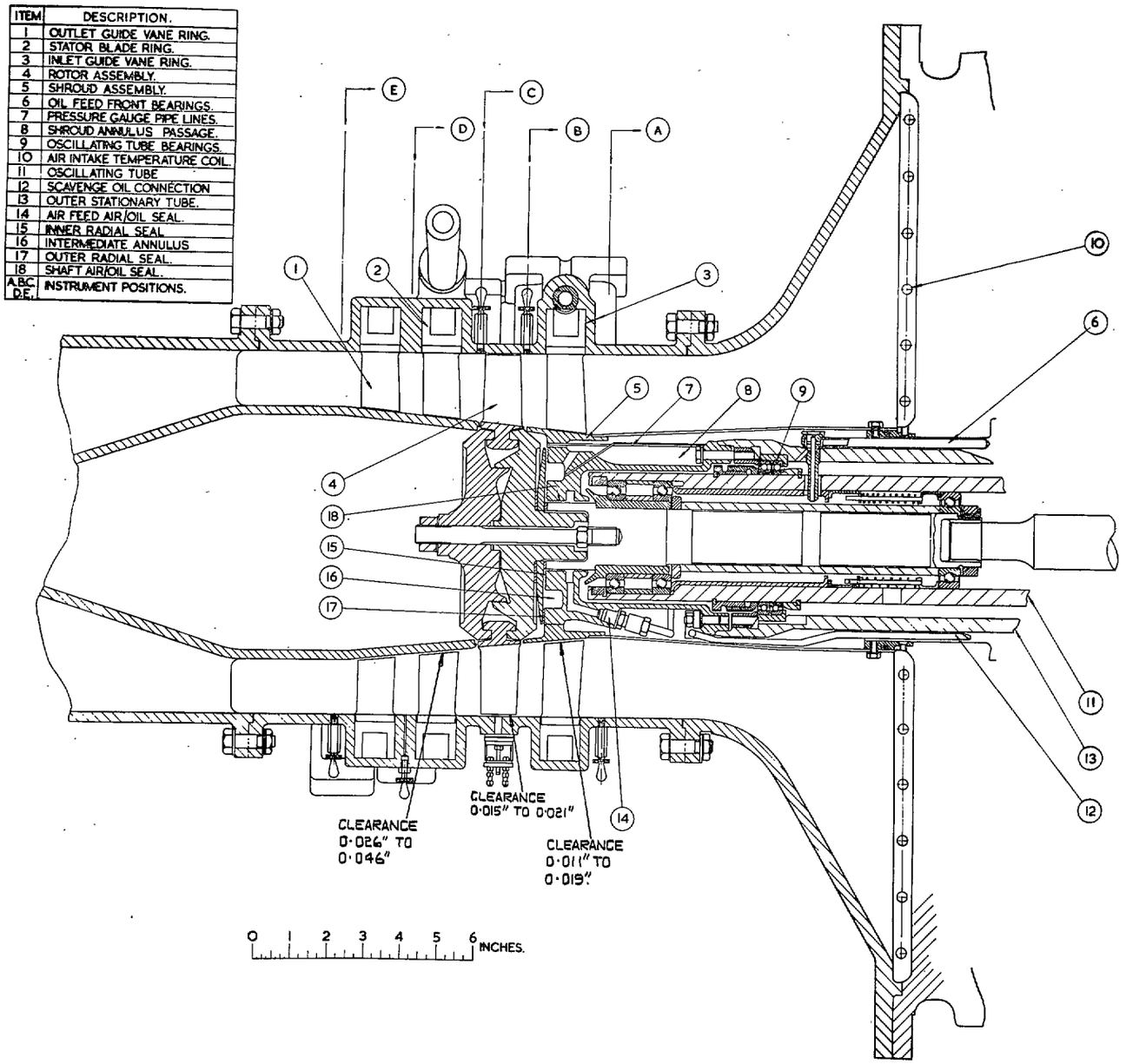

FIG. 2. Model compressor and drive.

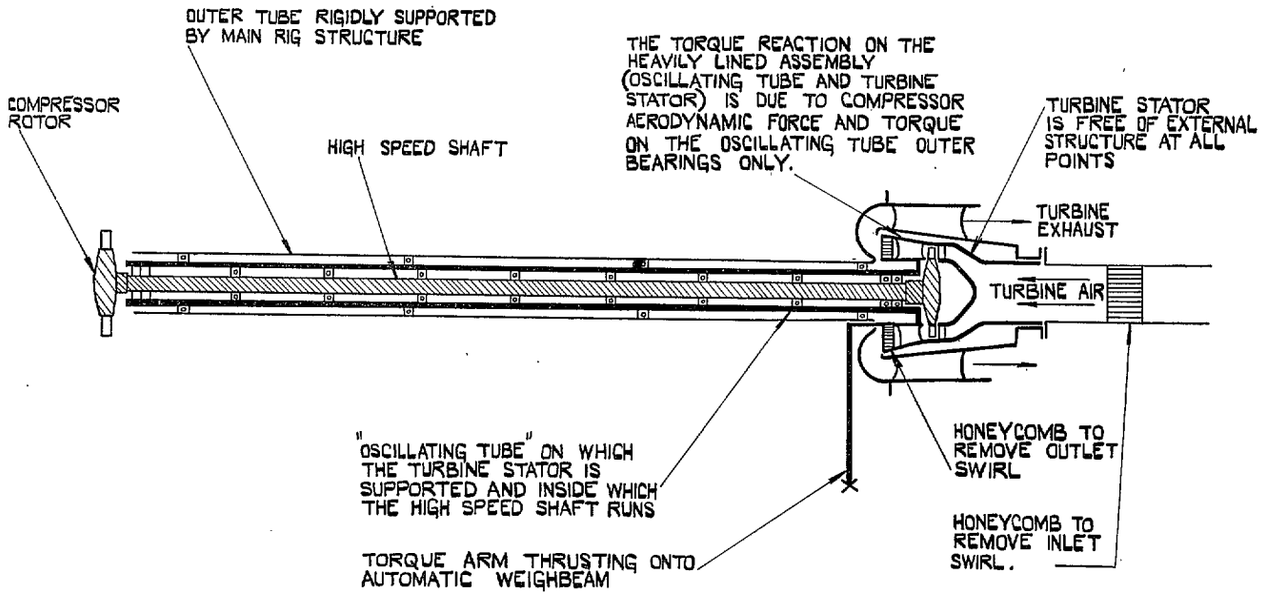

FIG. 3. Diagram showing principle of torque measurement.

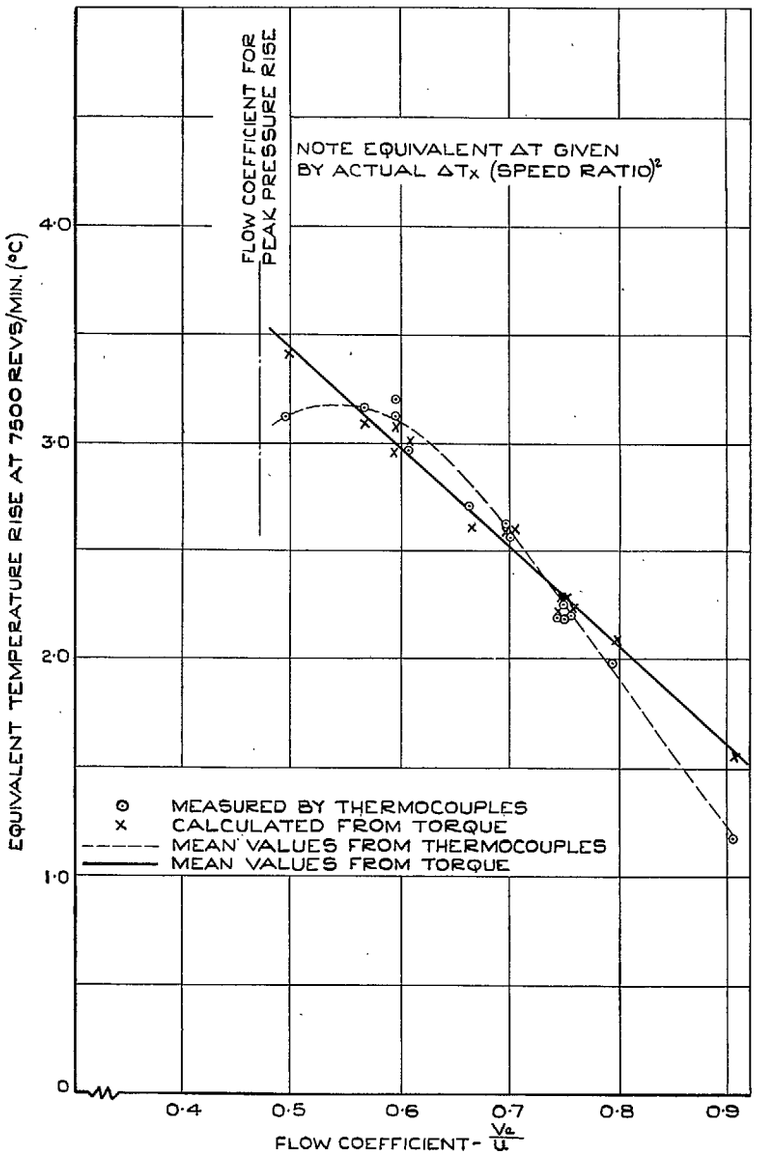

FIG. 4. Comparison of temperature measurements.

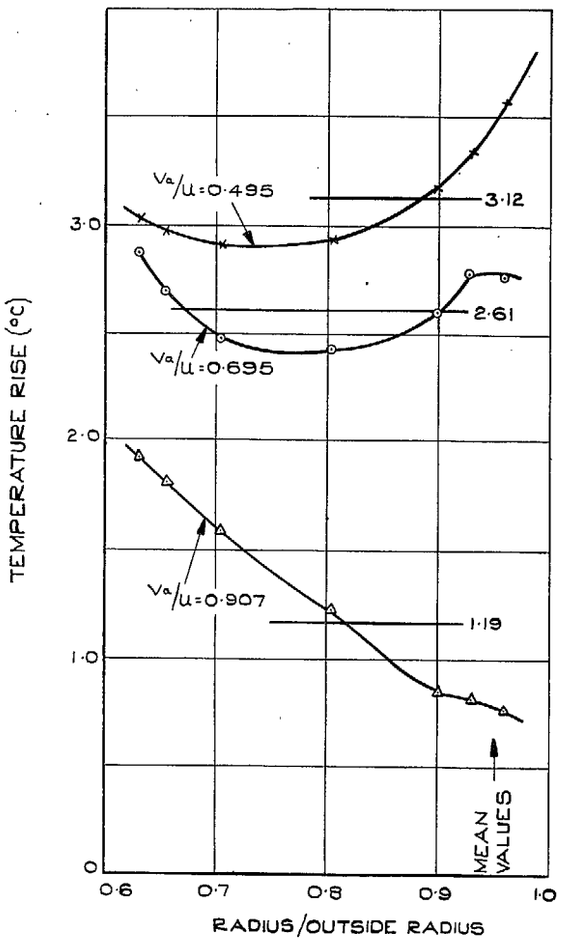

COMPRESSOR SPEED 7·500 REV/MIN.
RIG PRESSURE 1 ATMOSPHERE (NOMINAL)

FIG. 5. Radial variation of temperature rise.

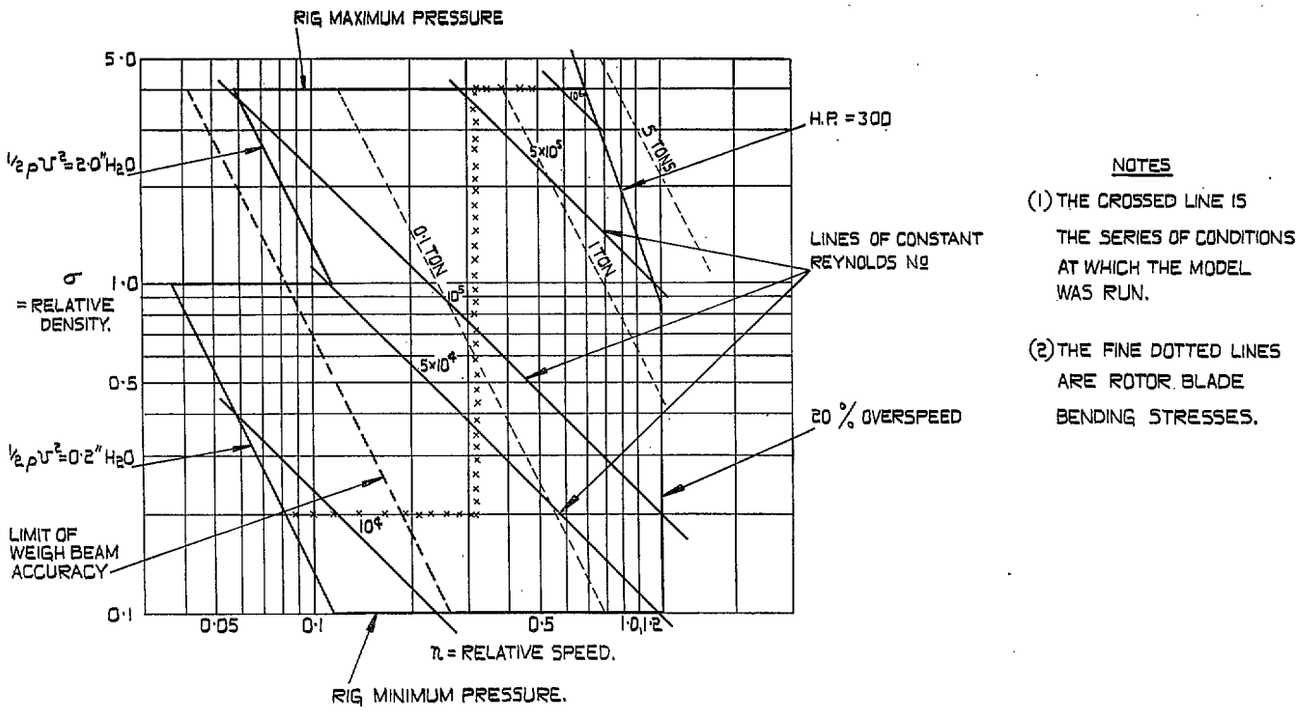

FIG. 6. Running condition envelope for 114 first test model.

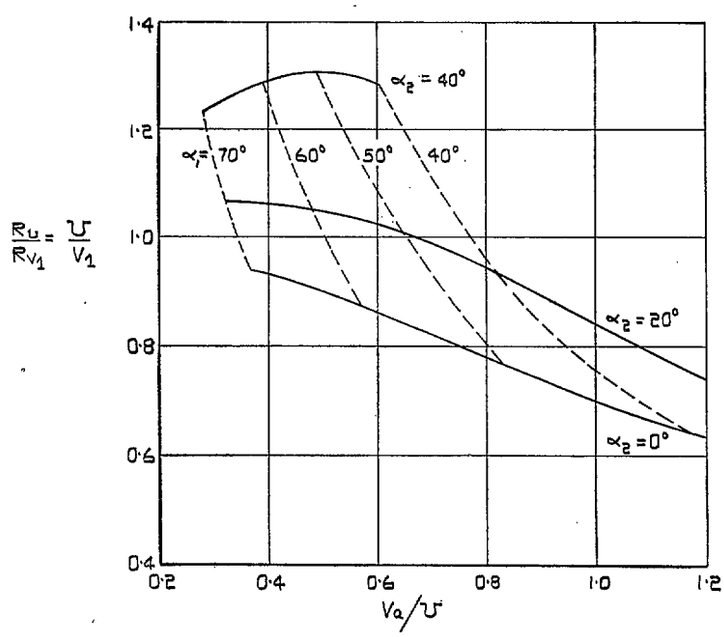

FIG. 7. Relation between R_U and R_{V1} for various α_2 and V_a/U for 50 per cent reaction stages.

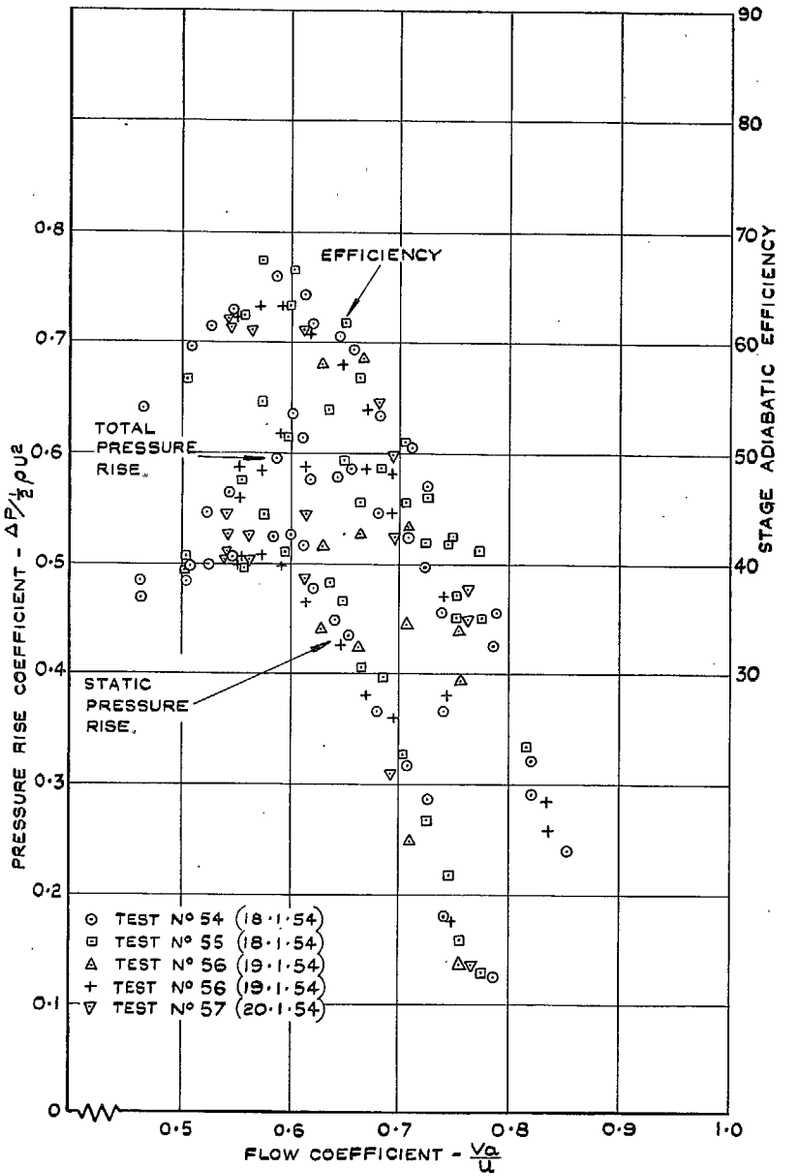

FIG. 8. Constant-speed stage characteristics. Reynolds number $0{\cdot}09 \times 10^5$.

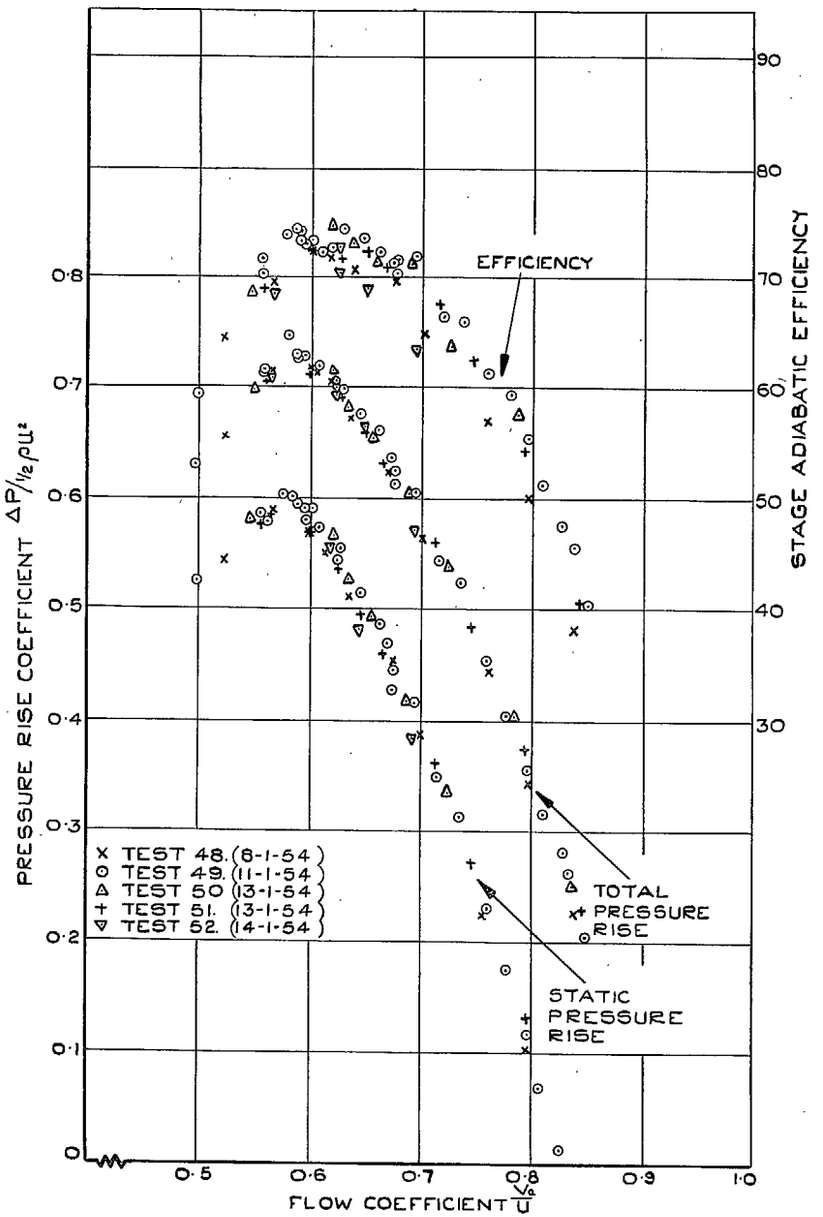

FIG. 9. Constant-speed stage characteristics. Reynolds number $0{\cdot}18 \times 10^5$.

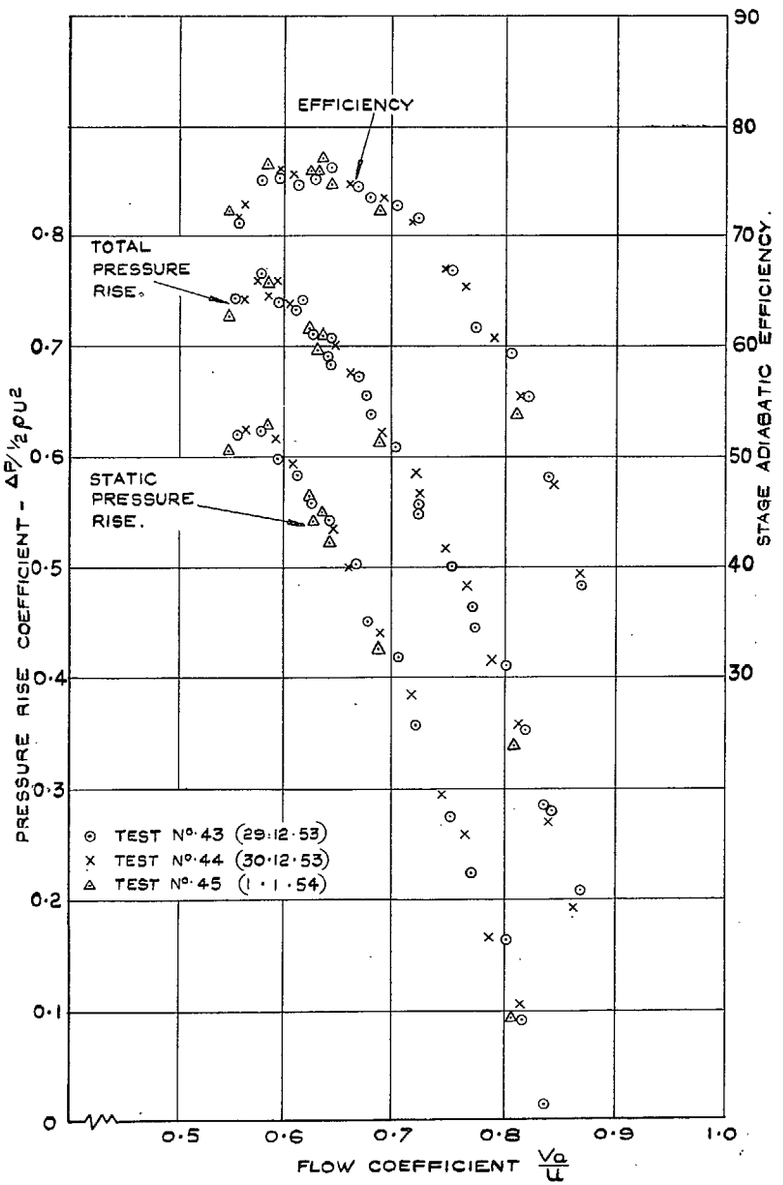

FIG. 10. Constant-speed stage characteristics. Reynolds number $0{\cdot}24 \times 10^5$.

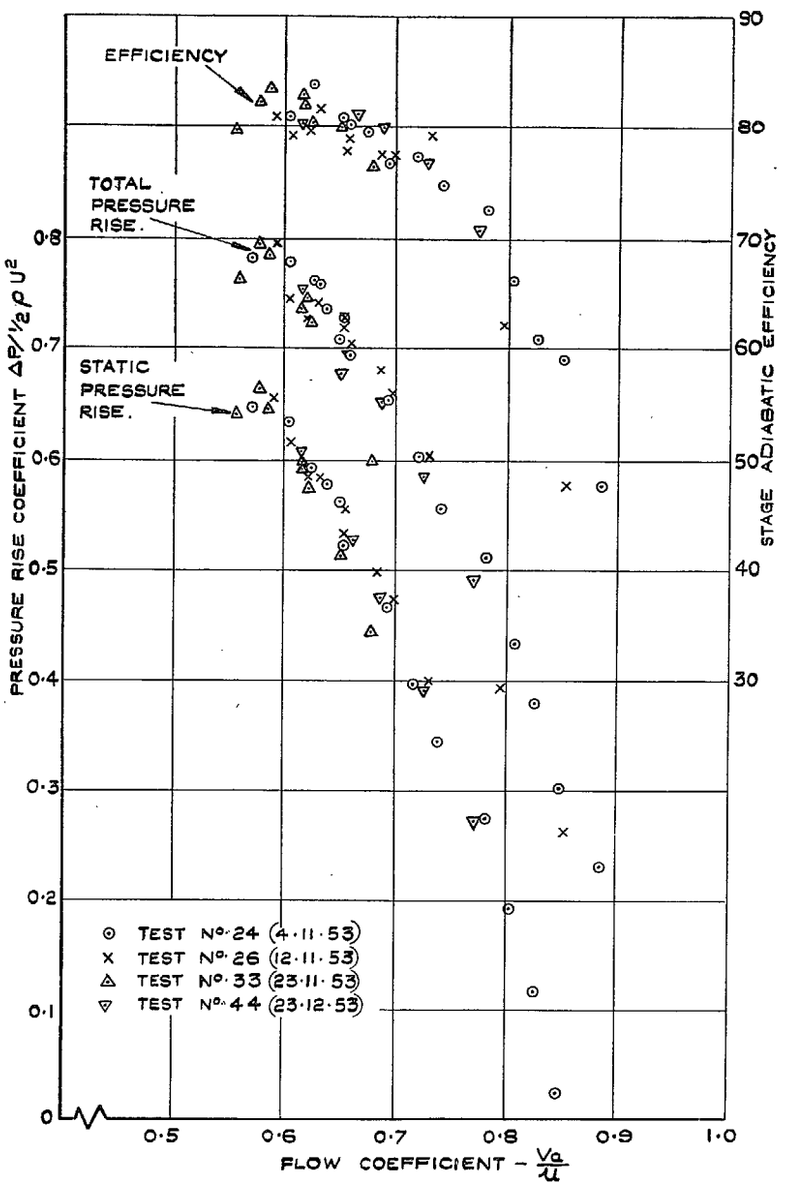

FIG. 11. Constant-speed stage characteristics. Reynolds number $0{\cdot}36 \times 10^5$.

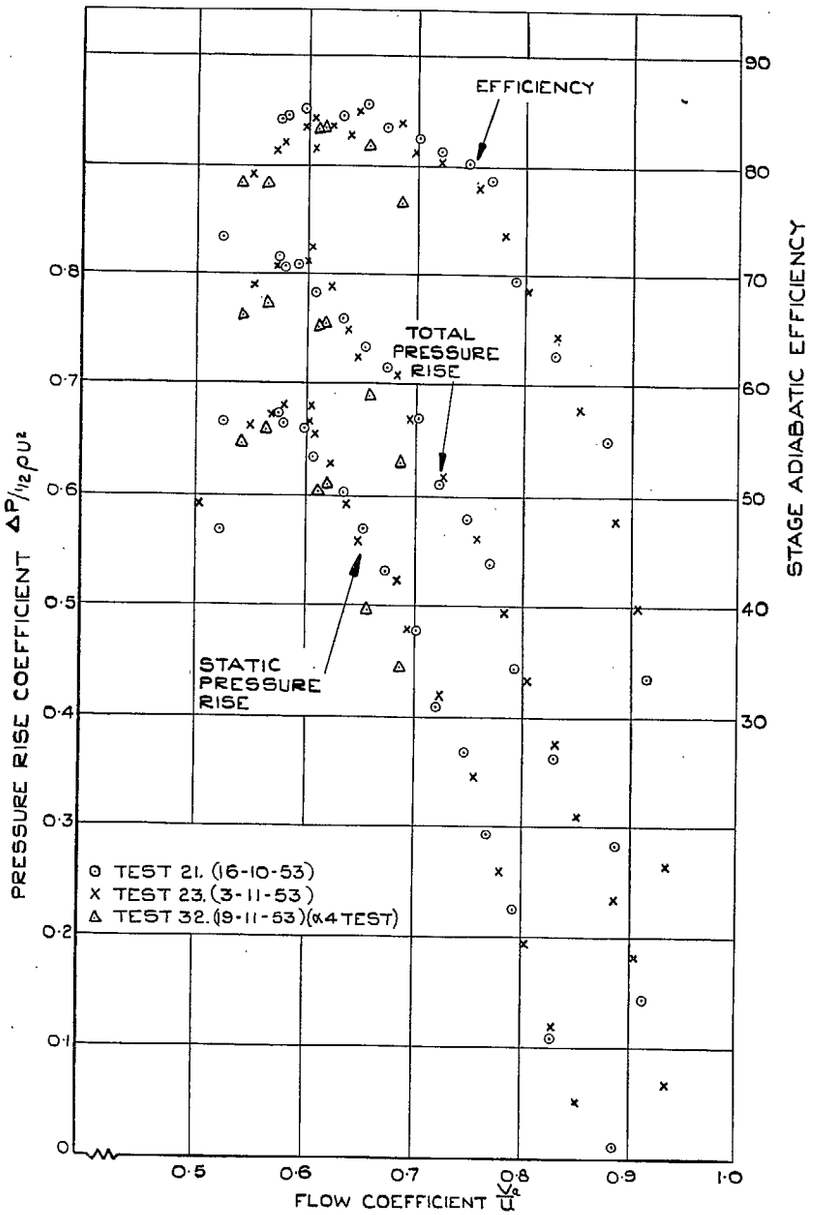

FIG. 12. Constant-speed stage characteristics. Reynolds number $0{\cdot}50 \times 10^5$.

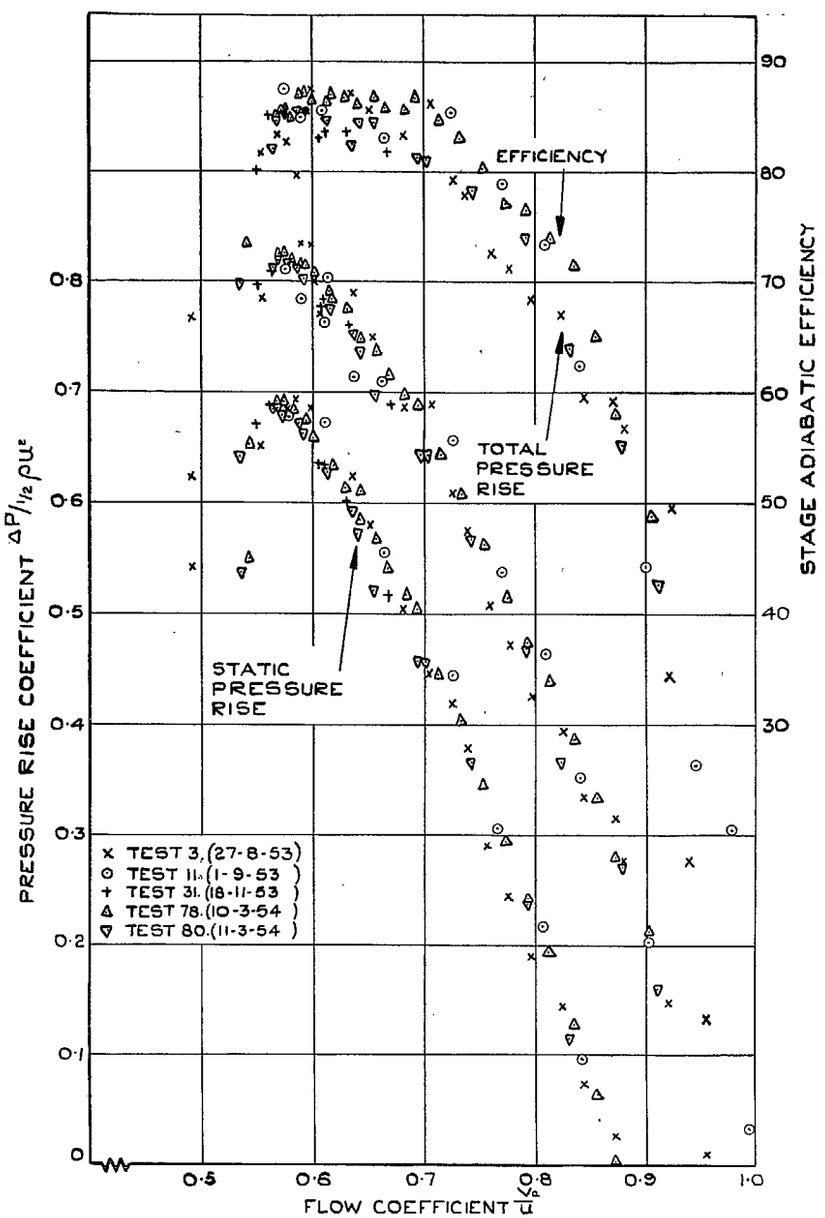

FIG. 13. Constant-speed stage characteristics. Reynolds number $0{\cdot}69 \times 10^5$.

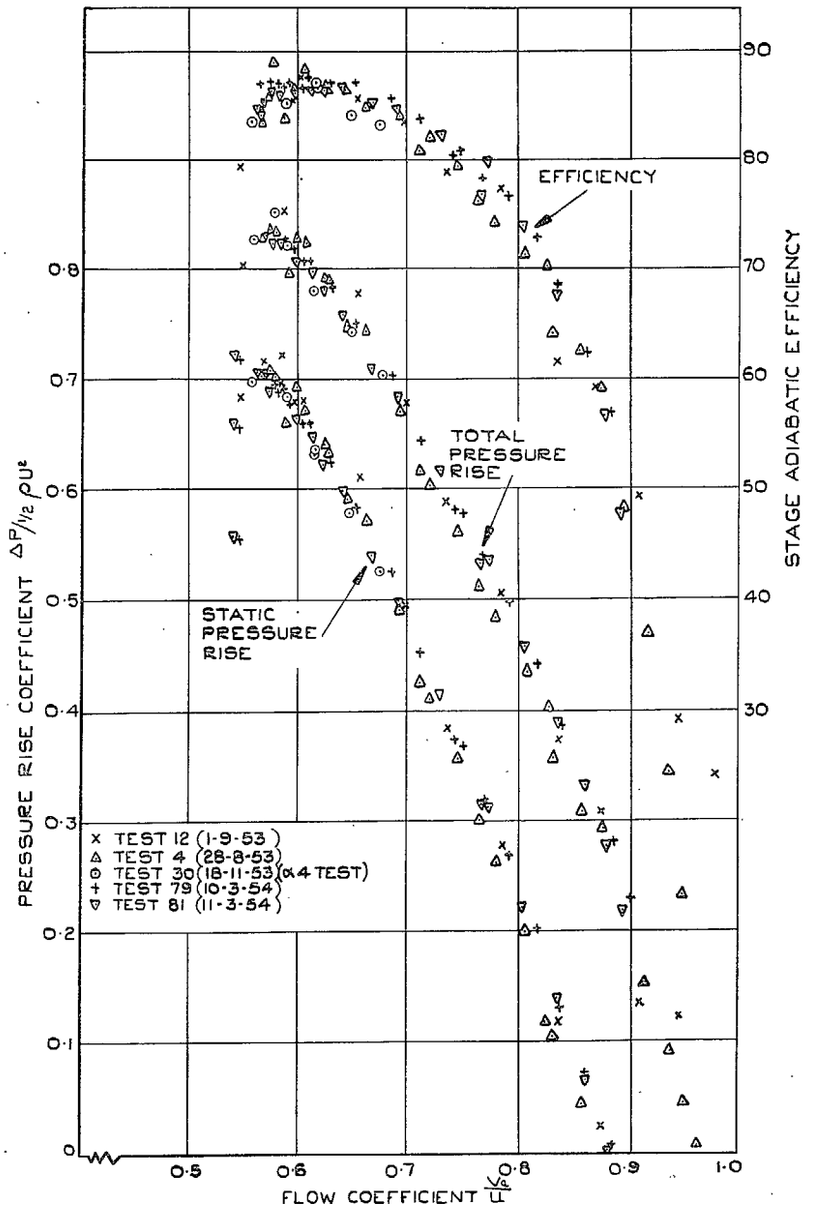

FIG. 14. Constant-speed stage characteristics. Reynolds number $0{\cdot}97 \times 10^5$.

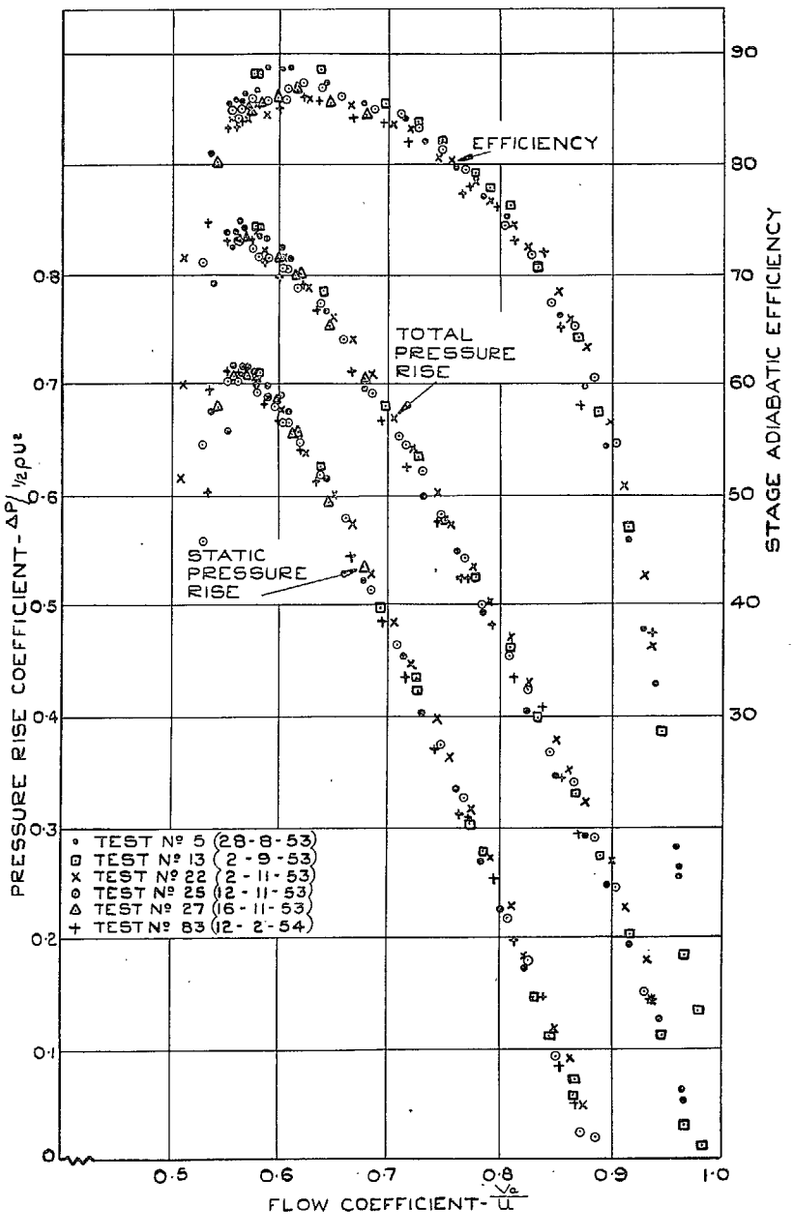

FIG. 15. Constant-speed stage characteristics. Reynolds number $1{\cdot}37 \times 10^5$.

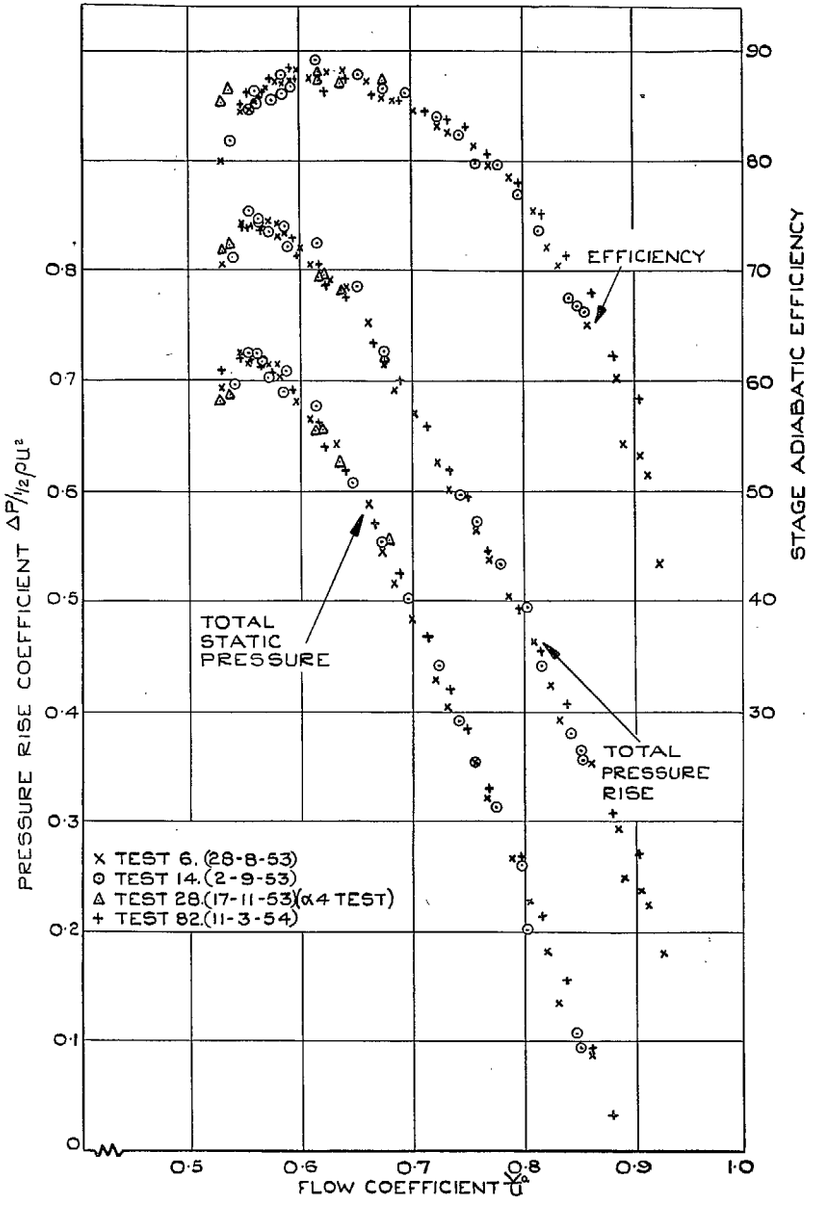

FIG. 16. Constant-speed stage characteristics. Reynolds number $1{\cdot}95 \times 10^5$.

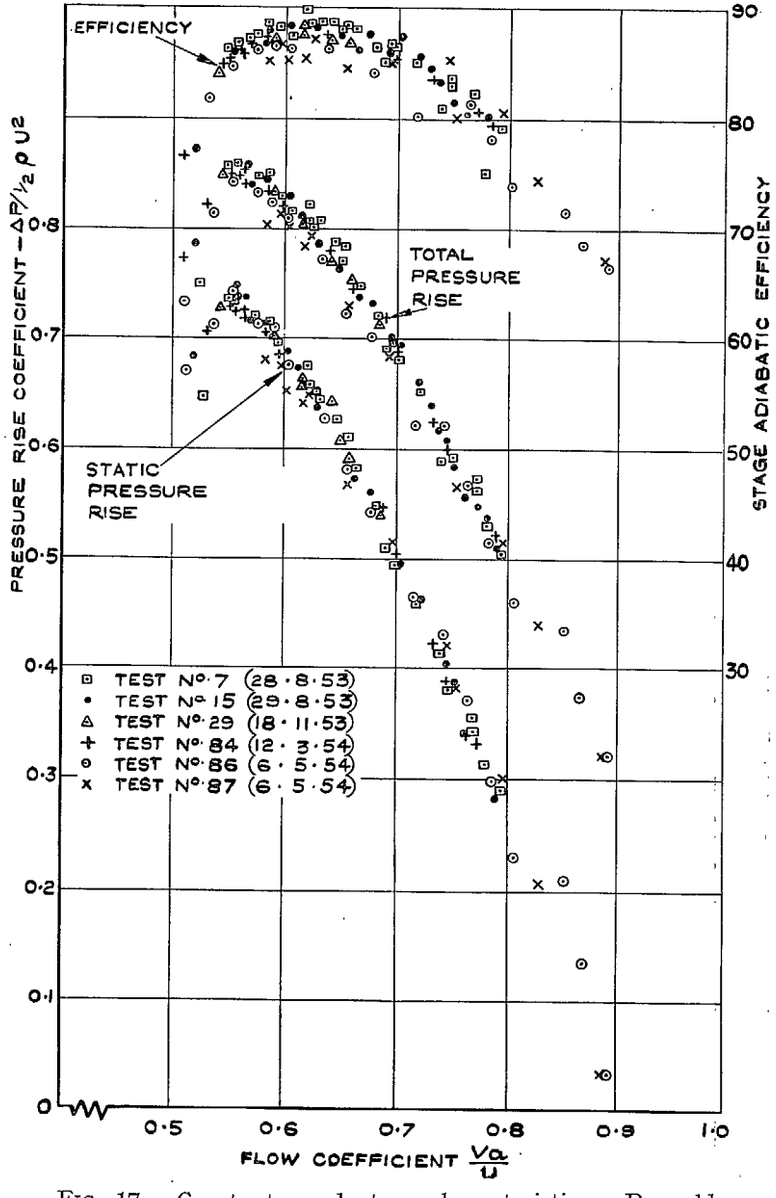

FIG. 17. Constant-speed stage characteristics. Reynolds number $2{\cdot}82 \times 10^5$.

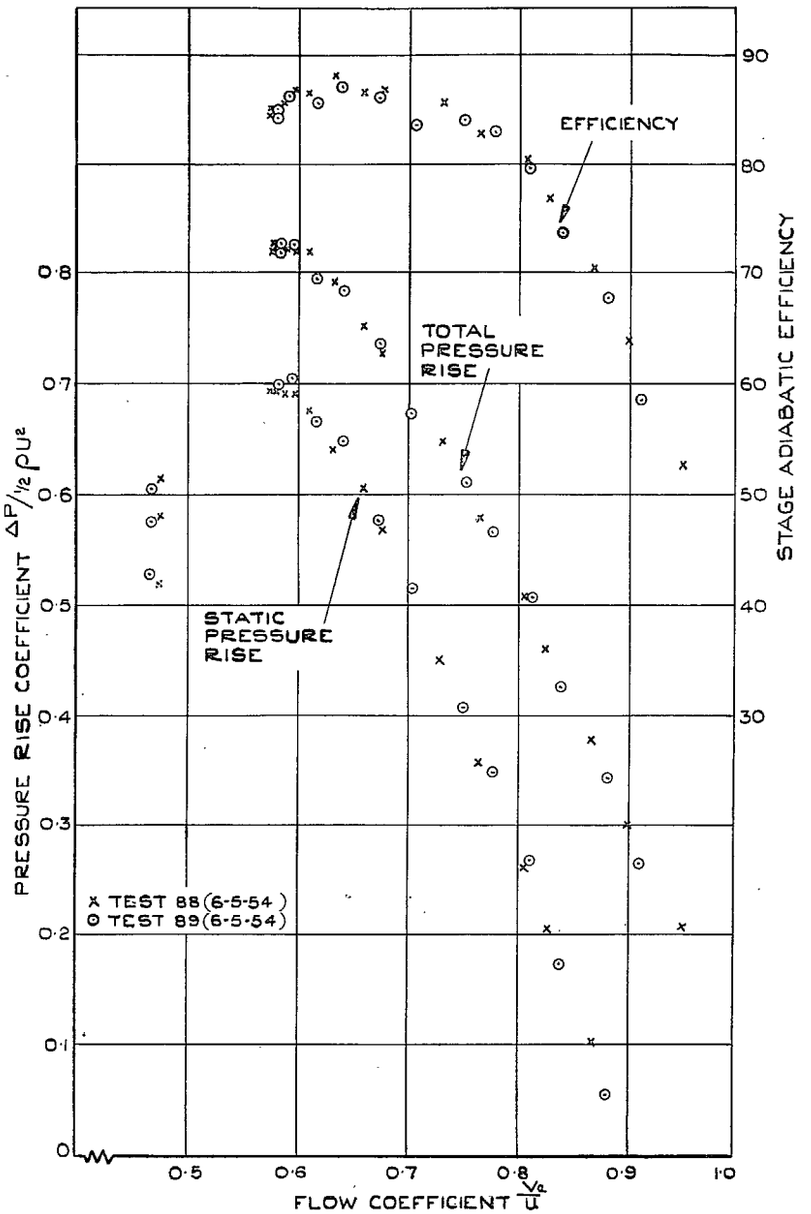

FIG. 18. Constant-speed stage characteristics. Reynolds number $3{\cdot}98 \times 10^5$.

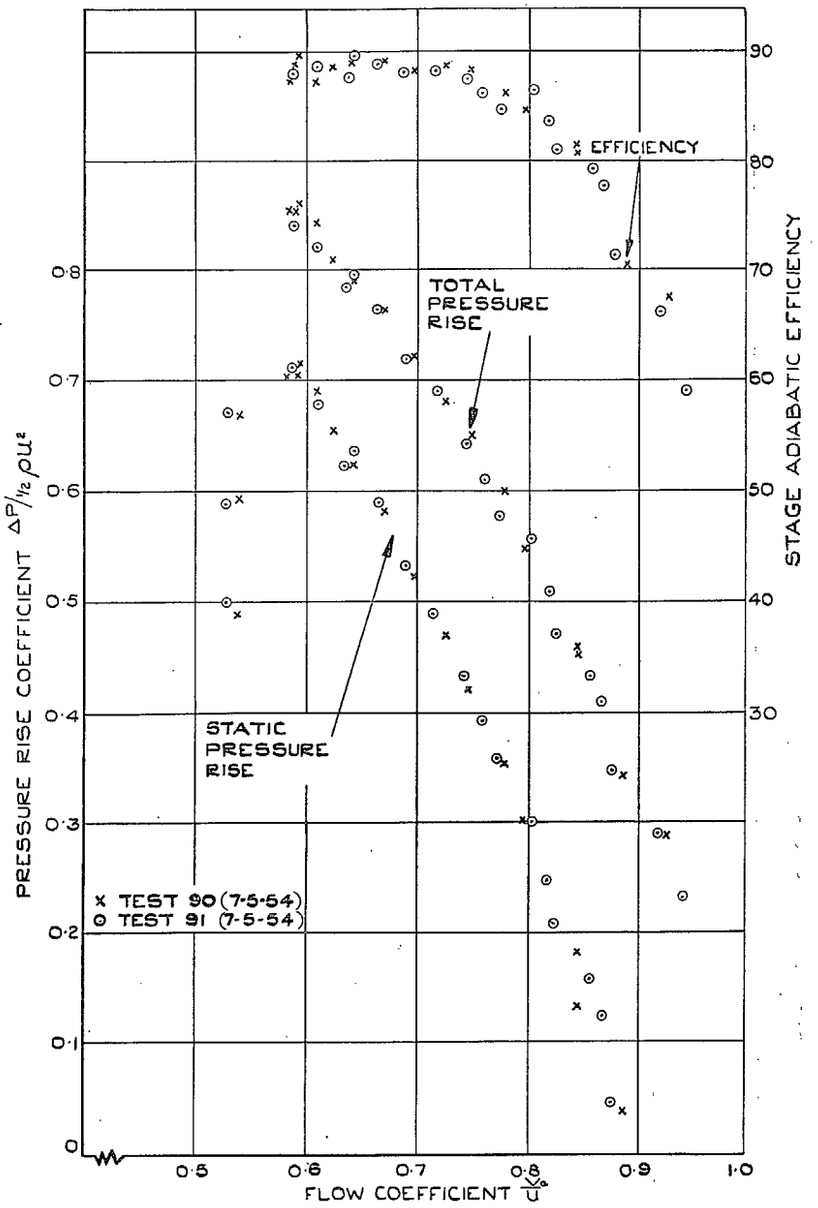

FIG. 19. Constant-speed stage characteristics. Reynolds number $5{\cdot}62 \times 10^5$.

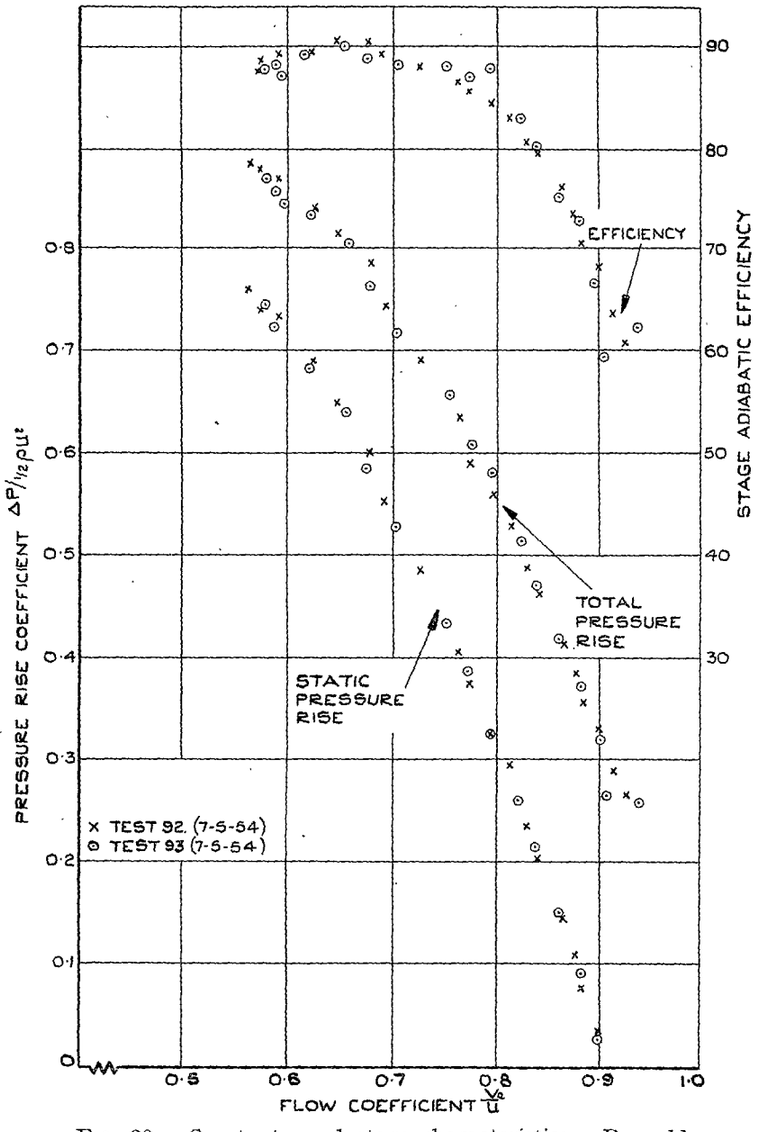

FIG. 20. Constant-speed stage characteristics. Reynolds number $7{\cdot}7 \times 10^5$.

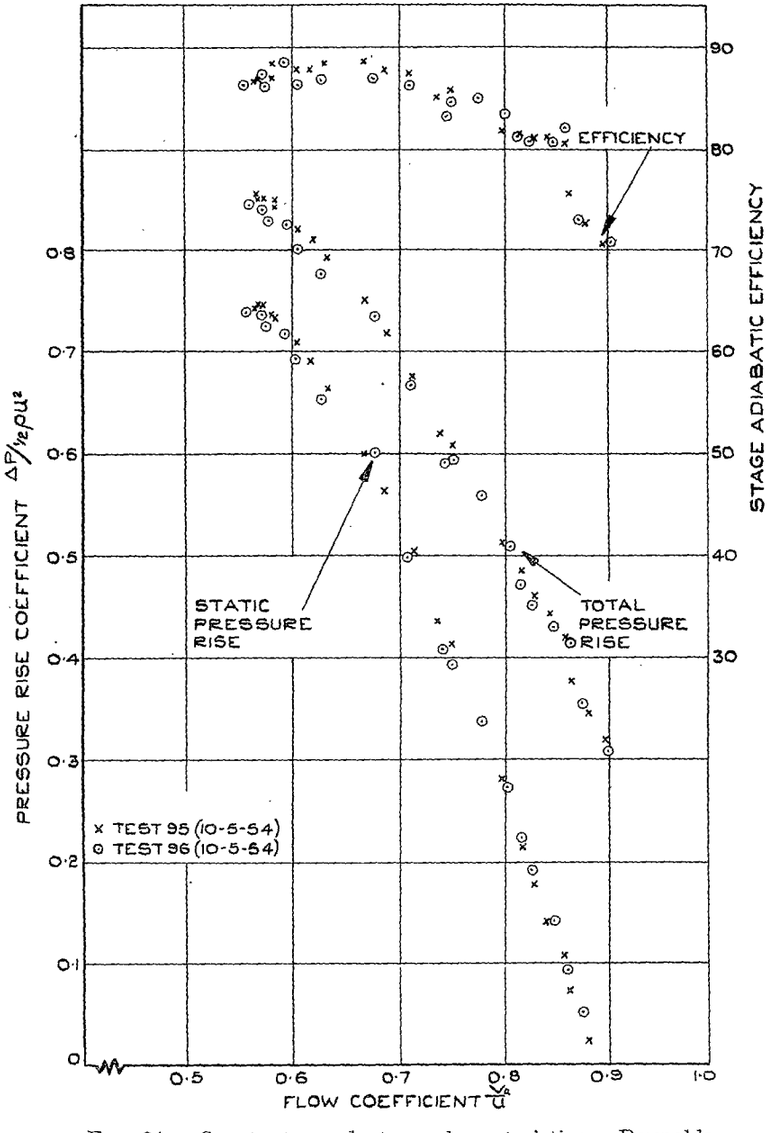

FIG. 21. Constant-speed stage characteristics. Reynolds number $8{\cdot}96 \times 10^5$.

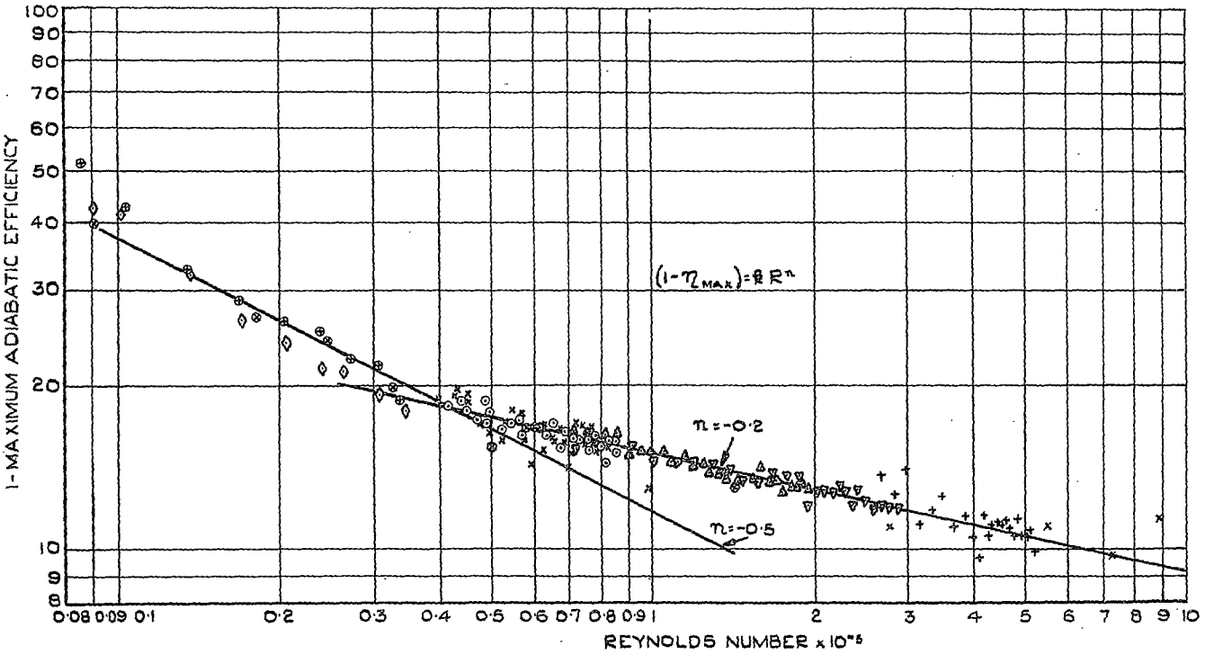

FIG. 22. Variation of peak stage efficiency.

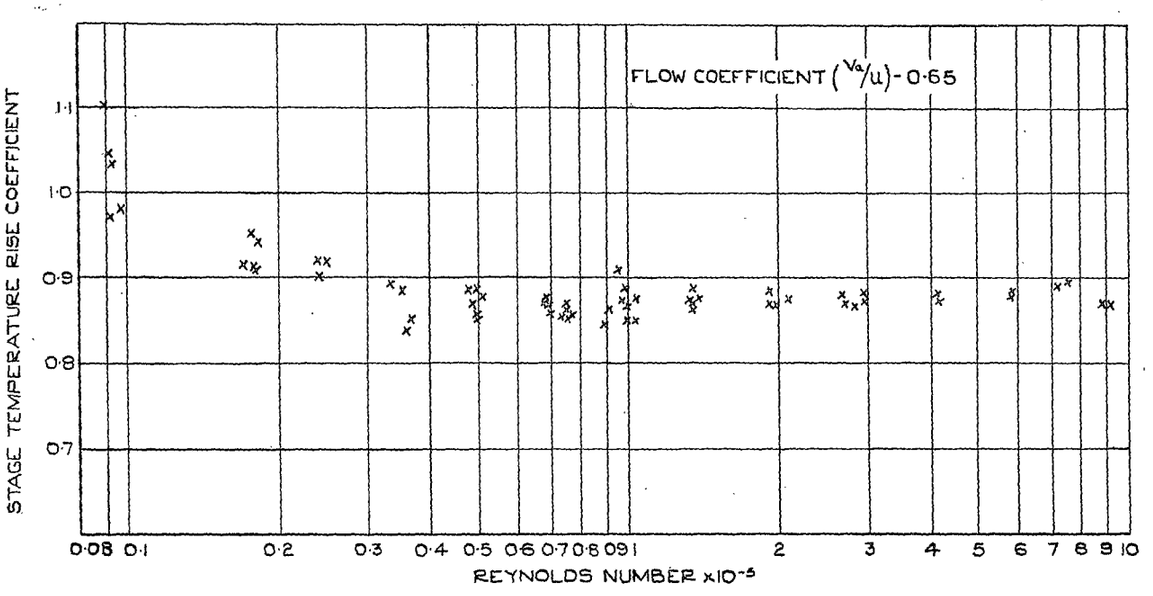

FIG. 23. Variation of stage temperature-rise coefficient.

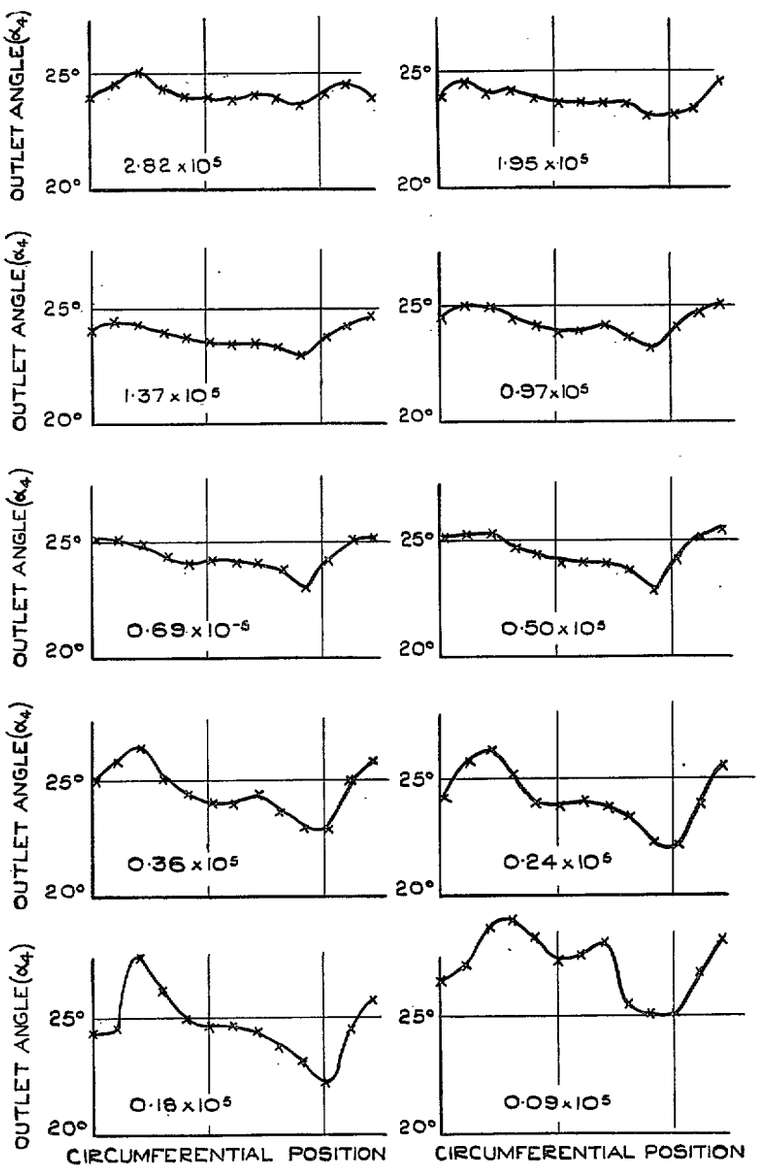

FIG. 24. Fluid outlet angle from stator.

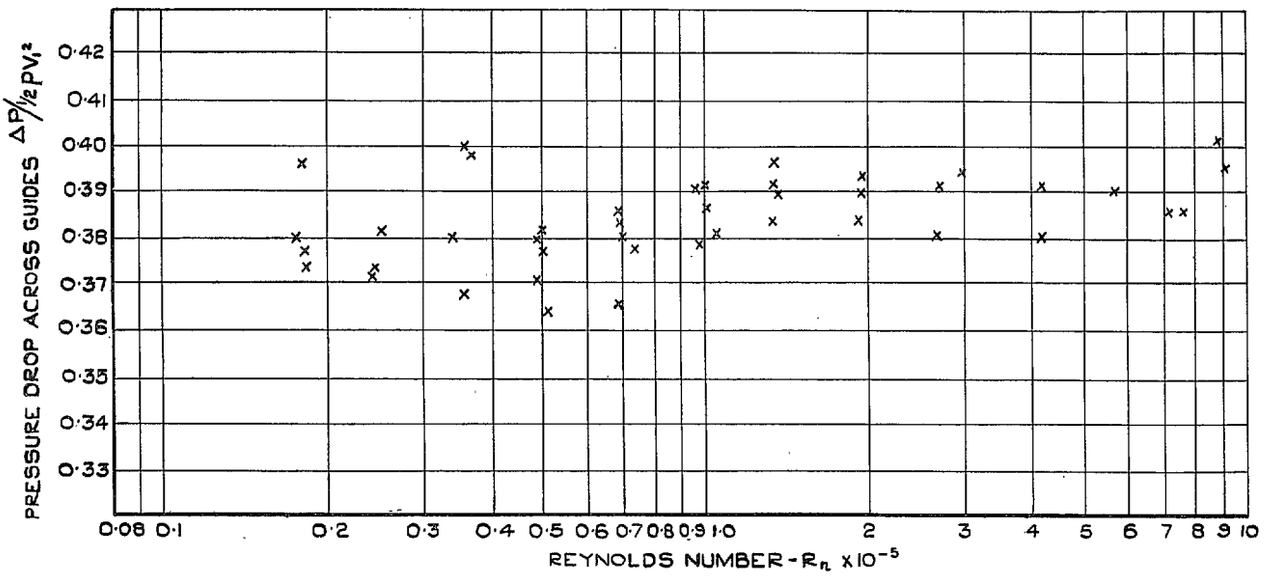

FIG. 25. Variation of static-pressure drop across inlet guides.

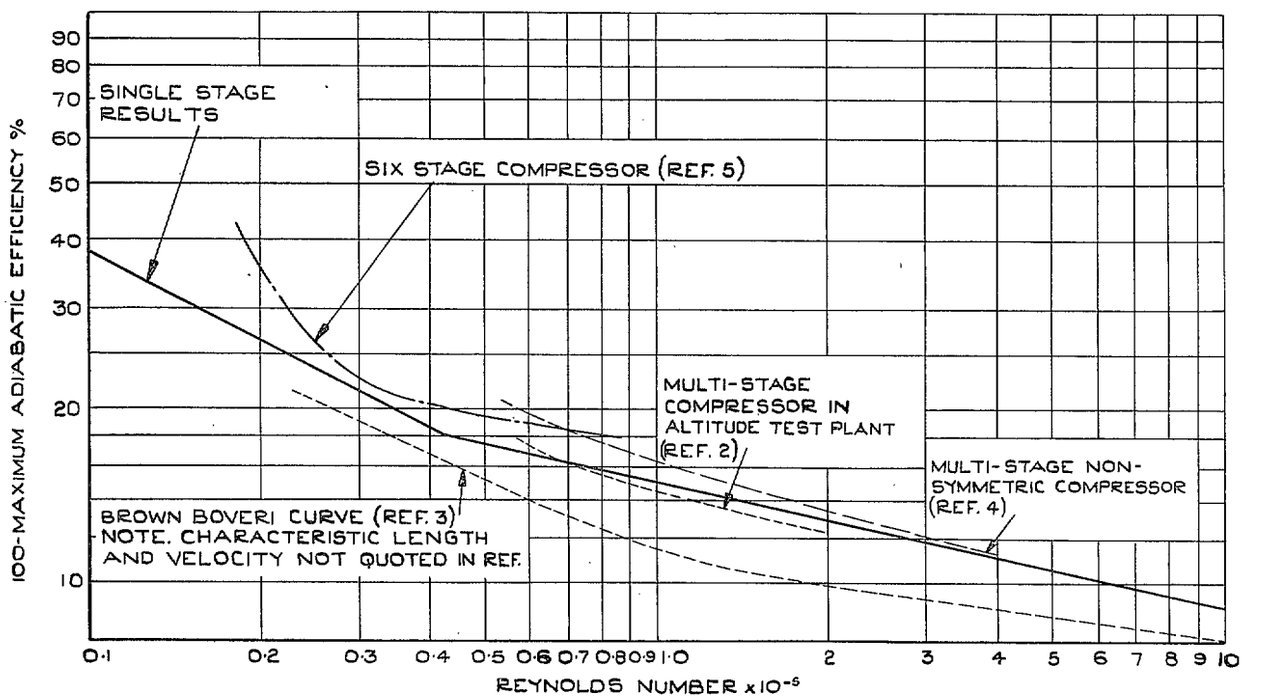

FIG. 26. Comparison with other results.

(80621) Wt. 61/991 K.7 11/60 Hw.

PRINTED IN ENGLAND

Publications of the Aeronautical Research Council

ANNUAL TECHNICAL REPORTS OF THE AERONAUTICAL RESEARCH COUNCIL (BOUND VOLUMES)

1939 Vol. I. Aerodynamics General, Performance, Airscrews, Engines. 50*s.* (52*s.*)
Vol. II. Stability and Control, Flutter and Vibration, Instruments, Structures, Seaplanes, etc. 63*s.* (65*s.*)

1940 Aero and Hydrodynamics, Aerofoils, Airscrews, Engines, Flutter, Icing, Stability and Control, Structures, and a miscellaneous section. 50*s.* (52*s.*)

1941 Aero and Hydrodynamics, Aerofoils, Airscrews, Engines, Flutter, Stability and Control, Structures. 63*s.* (65*s.* 3*d.*)

1942 Vol. I. Aero and Hydrodynamics, Aerofoils, Airscrews, Engines. 75*s.* (77*s.* 3*d.*)
Vol. II. Noise, Parachutes, Stability and Control, Structures, Vibration, Wind Tunnels. 47*s.* 6*d.* (49*s.* 3*d.*)

1943 Vol. I. Aerodynamics, Aerofoils, Airscrews. 80*s.* (82*s.*)
Vol. II. Engines, Flutter, Materials, Parachutes, Performance, Stability and Control, Structures. 90*s.* (92*s.* 3*d.*)

1944 Vol. I. Aero and Hydrodynamics, Aerofoils, Aircraft, Airscrews, Controls. 84*s.* (86*s.* 6*d.*)
Vol. II. Flutter and Vibration, Materials, Miscellaneous, Navigation, Parachutes, Performance, Plates and Panels, Stability, Structures, Test Equipment, Wind Tunnels. 84*s.* (86*s.* 6*d.*)

1945 Vol. I. Aero and Hydrodynamics, Aerofoils. 130*s.* (133*s.*)
Vol. II. Aircraft, Airscrews, Controls. 130*s.* (133*s.*)
Vol. III. Flutter and Vibration, Instruments, Miscellaneous, Parachutes, Plates and Panels, Propulsion. 130*s.* (132*s.* 9*d.*)
Vol. IV. Stability, Structures, Wind Tunnels, Wind Tunnel Technique. 130*s.* (132*s.* 9*d.*)

1947 Vol. I. Aerodynamics, Aerofoils, Aircraft. 168*s.* (171*s.* 3*d.*)

Annual Reports of the Aeronautical Research Council—

1939–48 3*s.* (3*s.* 5*d.*) 1949–54 5*s.* (5*s.* 5*d.*)

Index to all Reports and Memoranda published in the Annual Technical Reports, and separately—

April, 1950 - - - - R. & M. 2600 6*s.* (6*s.* 2*d.*)

Published Reports and Memoranda of the Aeronautical Research Council—

Between Nos. 2351–2449	R. & M. No. 2450 2*s.* (2*s.* 2*d.*)
Between Nos. 2451–2549	R. & M. No. 2550 2*s.* 6*d.* (2*s.* 8*d.*)
Between Nos. 2551–2649	R. & M. No. 2650 2*s.* 6*d.* (2*s.* 8*d.*)
Between Nos. 2651–2749	R. & M. No. 2750 2*s.* 6*d.* (2*s.* 8*d.*)
Between Nos. 2751–2849	R. & M. No. 2850 2*s.* 6*d.* (2*s.* 8*d.*)
Between Nos. 2851–2949	R. & M. No. 2950 3*s.* (3*s.* 2*d.*)

Prices in brackets include postage

HER MAJESTY'S STATIONERY OFFICE

York House, Kingsway, London W.C.2; 423 Oxford Street, London W.1; 13a Castle Street, Edinburgh 2; 39 King Street, Manchester 2; 2 Edmund Street, Birmingham 3; 109 St. Mary Street, Cardiff; 50 Fairfax Street, Bristol 1; 80 Chichester Street, Belfast 1, *or through any bookseller.*

S.O. Code No. 23-3184